PERFORMANCE OF DIAPHRAGM WALL CONSTRUCTED USING TOP-DOWN METHOD

By Chang-Yu Ou,[1] Member, ASCE, Jui-Tang Liao,[2] and Horn-Da Lin,[3] Member, ASCE

ABSTRACT: This paper presents the performance of an excavation using the top-down construction method. Strut loads, wall displacement, wall bending moment, ground surface settlement, pore-water pressure and bottom heave were measured. Results obtained from those observations are correlated with the construction activities. Field observations indicate that strut loads, wall displacement, and ground surface settlement correspond to those reported in the literature. Bending moments of the wall are studied based on the results of the rebar strain gauge and inclinometer measurements. The supported wall and the soil near the wall have a deep inward movement, which accounts for the magnitude of the lateral earth pressure acting on the wall. The behavior of the supported wall and soil over time is consistent with the variation of pore-water pressure during excavation. Analysis of excavations in soft clay should therefore consider the creep factors and/or pore-water pressure dissipation.

INTRODUCTION

Deep excavation in soft clay normally causes a large wall deflection and large ground surface settlement. Excessive ground surface settlement frequently damages the adjacent property in urban areas. The characteristics of wall deformation and ground movement must be thoroughly understood to protect the adjacent properties. Many investigators have provided studies of case histories, e.g., Karlsrud (1981), Mana and Clough (1981), and Ou et al. (1993), to understand these deformation characteristics. Furthermore, Finno et al. (1989) developed an extensive monitoring program on the Chicago subway excavation HDR-4 project. The observation items included surface and subsurface three-dimensional soil movements, pore-water pressures, sheet-pile deformations, and strut loads. The strength and stress-strain behaviors of the soil at the site were also studied thoroughly (Finno and Nerby 1989). In that case, high pore-water pressures were monitored during the sheet-pile driving, and very large ground movements were observed. This study enhances the knowledge of braced excavations in soft clay.

Most of the cases reported in the literature were constructed using the bottom-up excavation method. This method uses temporary steel struts to support the excavation wall. Installation of the struts requires a relatively short period of time (generally one to two weeks), depending on the size of the excavation. The displacement behavior of the supported wall and soil may change little during the period of strut installation because the pore-water pressure in the clay typically does not dissipate quickly. On the other hand, the top-down excavation method uses concrete floor slabs to support the wall and sometimes requires long periods of time between two successive excavation stages to construct the floor slab. Dissipation of excess pore-water pressure or creep behavior in the soil can have significant effects on the deformation behavior of the wall and soil. For these reasons, a comprehensive monitoring system was installed on the Taipei National Enterprise Center (TNEC) excavation project, which was completed using the top-down construction method. The TNEC structure is an 18-story building and has five basement levels. The site occupies an area of about 3,500 m^2, as shown in Fig. 1. This paper discusses strut loads, wall displacements, wall bending moments, ground movements, pore-water pressures, and bottom heaves associated with construction.

GROUND CONDITIONS

As shown in Fig. 2, the subsurface conditions at the site consist of six layers of alternating silty clay and silty sand deposits overlying a thick gravel formation. The first and second layers are a 5.6-m-thick silty clay (CL) and a 2.4-m-thick silty sand (SM), respectively. The third layer is a 25-m-thick silty clay (CL), and it is mainly this layer that affects the excavation behavior in this case. The liquid limit for this layer of clay ranges from 29 to 39, and the plastic index ranges from 9 to 19. The silt and clay contents are in the range of 40% to 55% and 45% to 60%, respectively. The coefficient of permeability (k) from one-dimensional consolidation tests is around 4×10^{-6} cm/s. The coefficient of consolidation (c_v) ranges between 3×10^{-3} cm^2/s and 1.1×10^{-3} cm^2/s. The fourth and fifth layers are a 2-m-thick medium dense fine sand and 2.5-m-thick medium to stiff clay. The sixth layer is an 8.0-m-thick medium to dense silt or silty sand. A gravel formation is located 46 m below the ground surface and has a standard penetration resistance N value greater than 328 blows/m.

Fig. 3 shows variation of water content, effective overburden pressure, and preconsolidation pressure with depth. The preconsolidation pressure appears to correspond well with the water content. The undrained shear strength was obtained from unconsolidated-undrained (UU) triaxial tests, field vane shear (FV) tests, triaxial K_0-consolidated undrained compression ($CK_0U - AC$) tests, and extension tests ($CK_0U - AE$), as shown in Fig. 4. The drained friction angle (ϕ') equals 30°. In addition, three cone penetration tests with pore-water pressure measurement (CPTU) were performed at the site. The variation in undrained shear strength computed using the formula provided by Roberston and Campanella (1989) from one of the CPTU tests is also shown in Fig. 4, in which the empirical cone factor, N_k, is equal to 15.

Because creep behavior of the silty clay may affect excavation behavior, a series of triaxial compression and lateral extension creep tests was conducted. Both types of these were consolidated isotropically prior to the creep test. Singh and Mitchell's parameters (1968), such as A_1, m, and α, can be obtained from the regression analysis of the test results. The results of the tests indicate that the parameters obtained from lateral extension creep tests are close to those from compression creep tests. This finding implies that the parameters from the compression creep test can be used in the excavation analysis while considering the creep effects, in which lateral de-

[1]Prof., Dept. of Constr. Engrg., National Taiwan Univ. of Sci. and Technol., Taipei, Taiwan, Republic of China.
[2]Grad. Student, Dept. of Constr. Engrg., National Taiwan Univ. of Sci. and Technol., Taipei, Taiwan, Republic of China.
[3]Prof., Dept. of Constr. Engrg., National Taiwan Univ. of Sci. and Technol., Taipei, Taiwan, Republic of China.

Note. Discussion open until February 1, 1999. To extend the closing date one month, a written request must be filed with the ASCE Manager of Journals. The manuscript for this paper was submitted for review and possible publication on February 8, 1996. This paper is part of the *Journal of Geotechnical and Geoenvironmental Engineering*, Vol. 124, No. 9, September, 1998. ©ASCE, ISSN 1090-0241/98/0009-0798–0808/ $8.00 + $.50 per page. Paper No. 12572.

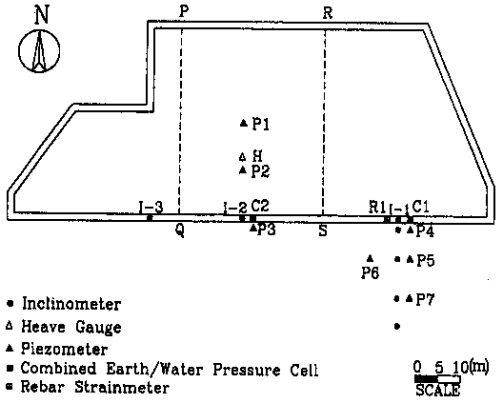

FIG. 1. Instrumentation Plan

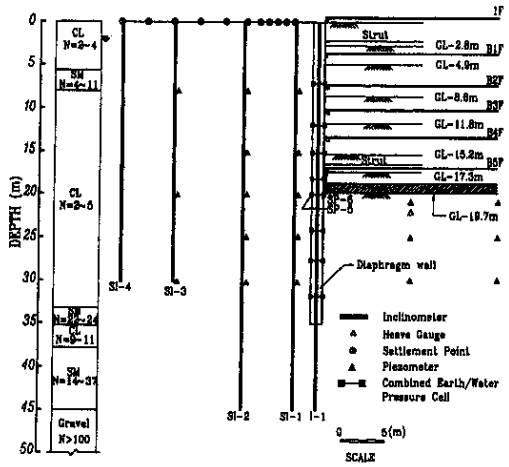

FIG. 2. Instrumentation Section

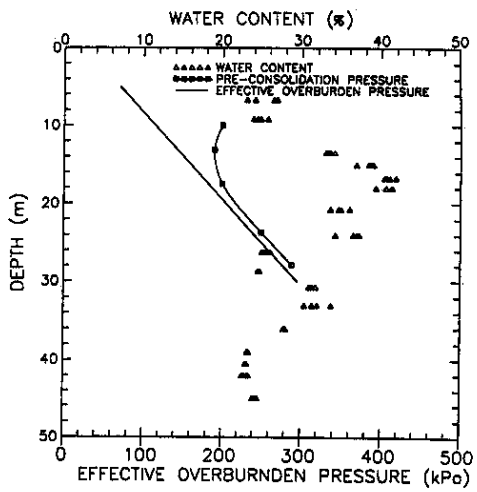

FIG. 3. Variations of Water Content, Preconsolidation Pressure, and Effective Overburden Pressure with Depth

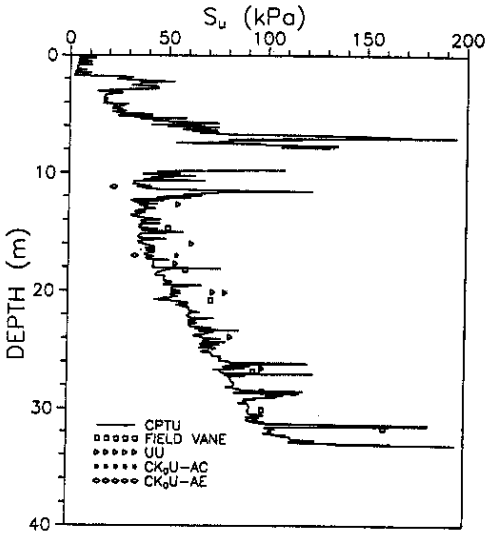

FIG. 4. Variation of Undrained Shear Strength

formation behavior is largely involved. Based on the test results, average A_1, m, and α are equal to about 0.0037, 0.94, and 5.04, respectively. Because m is smaller than 1.0, the in situ silty clay can be classified as having low to medium creep potential. The coefficient of secondary compression (ϵ_α) ranged from 0.48% to 0.6%. According to Mesri (1973), the soil can thus be classified as having low to medium secondary compressibility.

CONSTRUCTION SEQUENCE AND INSTRUMENTATION

Fig. 1 shows the excavation site along with the monitoring locations. As shown in this figure, the shape of the excavation site is slightly irregular. A 90-cm-thick and 35-m-deep diaphragm wall was used as the earth-retaining structure. The final excavation depth was 19.7 m, and was completed using the top-down construction method.

As indicated in Fig. 2, inclinometer casings I-1, I-2, and I-3 were installed in the wall, and SI-1 to SI-3 were installed along the main observation section outside the excavation zone. In the main observation section, the settlement measurement points were positioned at 1.0 m spacings at a distance from 2.0 to 7.5 m away from the wall and at 1.5 to 3.0 m spacings at distances of 7.5 to 49 m from the wall. This arrangement allowed the settlement profile to be continuously measured.

Fig. 2 also indicates that 16 combined earth/water pressure cells (eight on the back and eight on the front) were installed on a panel of the diaphragm wall in the main observation section at eight different depths. Six piezometers were also installed inside the excavation. Outside the excavation, piezometers were installed at various depths at five locations (P3 to P7), and P4 to P7 were arranged along the main observation section.

Stresses in the reinforced steel of the supported wall were measured by rebar strain gauges. Sixteen rebar strainmeters

TABLE 1. Excavation Sequence of TNEC Case History

Stage (1)	Interval (d) (2)	Construction activities (3)
	1–89	Construct diaphragm wall
	90–155	Construct pile foundation
1	156–162	Excavate to elevation of −2.80 m
2	164–169	Install H300 × 300 × 10 × 15 sections at first strut level (elevation of −2.0 m), preload = 784.8 kN per strut
3	181–188	Excavate to elevation of −4.9 m
4A	217	Cast floor slab (B1F) at elevation of −3.5 m
4B	222–328	Demolish first level of the strut and cast ground level of slab
5	233–255	Excavate to elevation of −8.6 m
6	279	Cast floor slab (B2F) at elevation of −7.1 m
7	318–337	Excavate to elevation of −11.8 m
8	352	Cast floor slab (B3F) at elevation of 10.3 m
9	363–378	Excavate to elevation of −15.2 m
10	400	Cast floor slab (B4F) at elevation of −13.7 m
11A	419–423	Excavate to elevation of −17.3 m (center strip)
12A	425–429	Install H400 × 400 × 13 × 21 sections at second strut level (elevation of −16.5 m), preload = 1,177 kN per strut (center strip)
11B	430–436	Excavate to elevation of −17.3 m (side strips)
12B	437–444	Install H400 × 400 × 13 × 21 sections at second strut level (elevation of −16.5 m), preload = 1,177 kN per strut (side strips)
13	445–460	Excavate to elevation of −19.7 m
	457	Complete the superstructure
14	464–468	Cast the foundation slab
15	506–520	Cast floor (B5F) slab at elevation of −17.1 m
16	528	Demolish second level of the strut

(eight on the back and eight on the front) were installed in the main observation section, as shown in Fig. 1.

As listed in Table 1, two levels of the struts were installed at some stages. To monitor the strut loads, vibrating wire strain gauges were attached on both sides of the web of the steel strut. The load in the strut could then be calculated on the basis of the measured strain.

Table 1 also presents the time sequence of construction activities for this project. Construction of the concrete diaphragm wall commenced on August 13, 1991. For the convenience of describing construction activities, the construction days are numbered starting from this day. As revealed in Table 1, stages 1, 3, 5, 7, 9, 11A, 11B, and 13 represent excavation stages, and stages 2, 4, 6, 8, 10, 12A, 12B, 14, and 15 represent stages for strut installation or concrete floor slab construction. To reduce the wall displacement, the excavation was carried out with zoning after the concrete floor slab (B4F) located at an elevation of −13.7 m was cast. During the zoned excavation, the center strip of the site (area PQRT in Fig. 1), was first excavated and then reinforced with the strut. Thereafter, the side strips of the site were excavated, and supported with the strut.

STRUT PERFORMANCE

For the first strut level, the horizontal strut spacing varied from 6.0 to 11.0 m, and was 8.0 m on average. The average nominal axial stiffness per unit width for the first strut level was 14,980 kN/m/m. The preloading force was 784.8 kN per strut, and was about 98.1 kN/m per unit width in the central region (i.e., plane strain condition). Because the preloading force can push the supported wall outward toward the unexcavated side and may damage adjacent buildings, the magnitude of wall movement usually is a concern in excavation design. Field observation results indicate that the preloading force appeared to have an insignificant effect on the wall deflection. This insignificant effect may be due to the relatively low preloading forces in the struts.

TABLE 2. Observed Strut Loads at Final Stage

Number (1)	Distance from corner* (m) (2)	Strut load (kN) (3)	Tributary width (m) (4)	Strut load per unit width (kN/m) (5)
SA-1	23 (W.C.)	853.5	4.0	213.4
SA-2	45 (W.C.)	2,324	3.1	749.5
SA-3	38 (E.C.)	1,813	2.5	725.0
SA-4	20 (E.C.)	1,525	3.7	412.0

*W.C. denotes western corner; E.C. denotes eastern corner.

After the floor slab, B1F, was cast, the strut was demolished. The force in the strut was released, which subsequently caused the wall to move inward. Under such a circumstance, the safety of the supported system was checked. Field observation results also indicate that demolishing the strut also had only a slight effect on the outward wall deflection.

At the second strut level, the horizontal strut spacing varied from 2.5 to 6.0 m, and averaged 3.0 m. The average nominal axial stiffness of the strut per unit width was 64,363 kN/m/m. The preloading force was 1,177 kN per strut, and was about 392 kN/m per unit width in the central region. The strut was demolished at day 528 after the floor slab, B5F, was completed. Field observation results indicate that preloading and demolishing the strut had no effect on the wall deflection. This may imply that the preloading force cannot overcome the lateral earth pressure acting on the wall at this stage.

The strain gauge was not installed on the first level of the strut because the load in this level of the strut was not expected to be large. For the second strut level, four sets of strain gauges were installed on the struts (SA-1, SA-2, SA-3 and SA-4) in the north-south direction. Table 2 lists the distance to the corner for these struts and the loads in the struts at the final stage of excavation. Since struts SA-1 and SA-4 were close to the corners, the corner effects apparently have a significant effect on the strut loads. Therefore, the data were excluded from the following analyses.

As indicated in Table 2, the loads in struts SA-2 and SA-3 per unit width, considered as the plane strain condition, were 750 kN/m and 725 kN/m, respectively. The average value was 737.5 kN/m. Because the apparent earth pressure envelopes available are only for uniform soil, questions may arise regarding how to treat the subsoil conditions shown in Fig. 2. Fig. 5 shows the apparent earth pressure envelopes proposed by Peck (1969), considering that the undrained shear strength was 58.6 kPa at the position of strut installation, i.e., an elevation of −16.5 m, and the average value of the soil within the depth of excavation, i.e., 19.7 m (Fig. 4), was 34.5 kPa. This figure reveals that the observed value was close to the computed value based on the average undrained shear strength in engineering practice.

DISPLACEMENT OF DIAPHRAGM WALL

Fig. 6 shows the horizontal displacement of the diaphragm wall at I-1, I-2, and I-3 at the final construction stage (stage 13). As indicated in this figure, the wall displacements at these inclinometers are similar. This finding exhibits that the wall at I-1, I-2, and I-3 is in the plane strain condition.

Figs. 7(a and b) show displacements of the diaphragm wall and transverse horizontal ground deformations in the main observation section after the completion of each excavation stage. As shown in Table 1, the site was first excavated down to 2.8 m below the ground surface (elevation −2.8 m). The strut was not installed and the floor slab was not constructed at this time. At the subsequent stage, the struts were installed at an elevation of −2.0 m; the site was then excavated down to 4.9 m. The nominal axial stiffness per unit width, 14,980

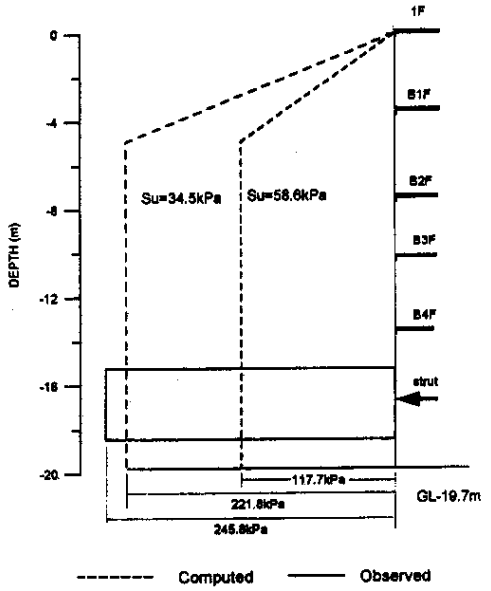

FIG. 5. Comparison of Observed Apparent Earth Pressure and Peck's Earth Pressure Envelope

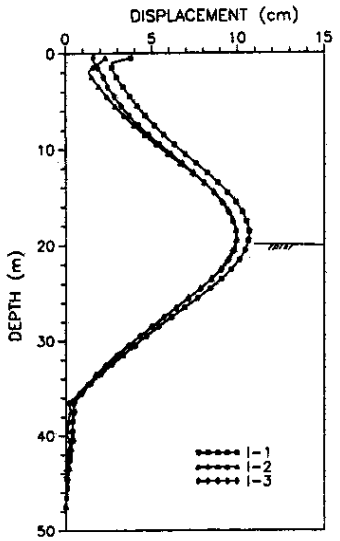

FIG. 6. Displacements of the Wall at Inclinometers I-1, I-2, and I-3 at Final Excavation Stage

kPa, which is considered relatively low, might not be able to prevent the wall movement. The wall and soil deformations at these two stages behaved as a cantilever, in which the maximum horizontal displacement occurred at the top level of the wall, as Fig. 7(a) shows.

As the excavation proceeded to stage 5 (excavation depth = 8.6 m), the surface level and the first level of the floor slab were constructed. The diaphragm wall rotated with respect to

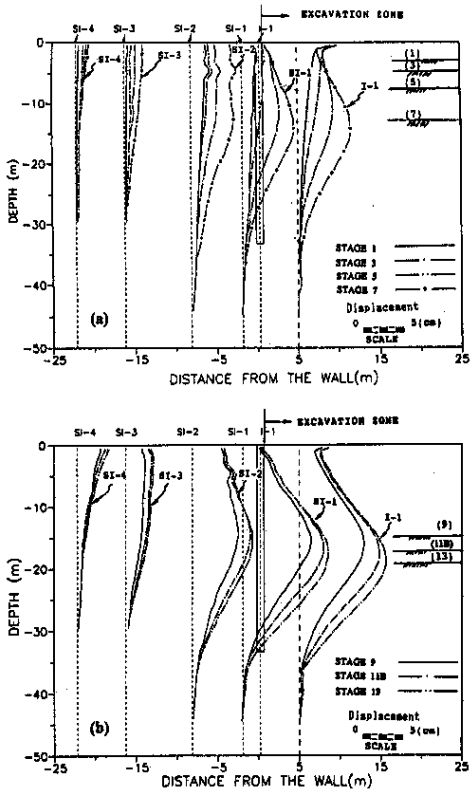

FIG. 7. Wall Displacement and Soil in the Main Observation Section, with the Location of I-1 Shown Inside Excavation for Illustration Purposes: (a) Stages 1–7; (b) Stages 9–13

the position of the floor slabs because the high axial stiffness of the slabs prevented the wall from moving at these positions. Deep inward movement thus developed on the wall, with the maximum wall displacement occurring near the excavation surface. Soil at SI-1 and SI-2 also had a deep inward type of movement. Soil at SI-3 and SI-4 continued to behave like a cantilever.

Deep inward movements continuously developed on the diaphragm wall for the subsequent construction stages. The amount of wall movements increased with excavation depth. The maximum wall deformation for each stage occurred near the excavation surface. Soil at SI-1 had a deformation pattern similar to that of the wall at all stages. Soil at SI-2 at stage 5 began to deform inwardly at a depth below the ground surface (deep inward movement), and the deformation became more pronounced after stage 9. Soil at SI-3 at stage 11B began to deform inwardly at a depth. Soil at SI-4 behaved like a cantilever at all stages.

As shown in Figs. 7(a and b), the maximum deformations of the wall were close to those of the soil at SI-1 at all stages. For instance, at stage 13 (excavation depth = 19.7 m), the maximum wall deformation was 10.6 cm; the maximum soil deformation at SI-1 was 10.5 cm. However, the horizontal deformation of the top level of the wall was obviously smaller than that of the ground surface at SI-1 at all stages. The line of the locations of maximum deformation at all inclinometer

casings (I-1, SI-1, SI-2, SI-3, SI-4) might be the potential failure surface. The ratios of maximum wall deformation to excavation depth for stages 1 and 3 were about 0.89%, where the maximum wall deformation occurred at the top level of the wall; the ratios for all other stages ranged from 0.51 to 0.57%, which are higher than the general trends found by Ou et al. (1993).

Fig. 8 shows the wall movements with time at different depths. As shown in this figure, the wall movement increased with time while the excavation depth remained unchanged. This is because the top-down construction generally requires considerable time to erect the mold and to pour the concrete floor slab before the next stage of excavation. Durations of 30 to 60 days were frequently encountered for the TNEC project, as shown in Table 1. Both soil creep and excess pore-water pressure dissipation may partially contribute to some extent.

Fig. 9(a) shows the relationship between the maximum deflection rate for the wall at I-1, I-2, and I-3 and the excavation depth. In this figure, the deflection rate ($\Delta\delta/\Delta t$) is defined as the ratio of deflection increment ($\Delta\delta$) to the period of the excavation depth remaining unchanged (Δt). Since an inclinometer casing has many measurement points and thus has many deflection rates for a given excavation depth, the maximum value of the deflection rate ($\Delta\delta/\Delta t$) was used to study the deformation behavior as a function of time. As shown in this figure, the maximum deflection rate generally increased with excavation depth. Except for stage 1 (excavation depth = 2.8 m), most of the maximum deflection rates were in the range of 0.1 mm/d to 0.6 mm/d.

Fig. 9(b) shows the relationship between the maximum deflection rate of inclinometer casings SI-1, SI-2, and SI-3 and the excavation depth. As indicated in this figure, the maximum deflection rates at SI-1 were close to those of the diaphragm wall. The maximum deflection rate at SI-4 remained nearly unchanged with time. The maximum deflection rate for the inclinometer casings decreased with increasing horizontal distance from the diaphragm wall. This is perhaps attributed to the fact that for a given depth, the stress level of the soil decreases with an increasing horizontal distance from the wall, with the stress level defined as the ratio of the principal stress difference to the soil strength. Higher values of the stress level of the soil normally have more pronounced creep behavior.

Table 3 lists the deflection of the diaphragm wall at depths of 10 and 20 m below the ground surface during the period when the excavation depth remained unchanged. Since the excavation after stage 10 was conducted with zoning, differentiating the deflection for the period when the excavation depth remained unchanged from the total deflection is difficult. Therefore, only deflection data from the beginning of excavation to the day of measurement before stage 10 (excavation depth = 15.2 m) are used in the table. The table shows that the accumulated deflections (δ_1) at the depths of 10 and 20 m during the periods when the excavation depths remained unchanged were 18.88 and 29.29 mm, respectively; the corresponding total deflections (δ_2) at these depths were 62.54 mm and 80.56 mm (Fig. 8), respectively. The percentages of accumulated deflection during the periods when the excavation depths remained unchanged, δ_1/δ_2, were 30% and 36%, respectively. These percentages were fairly large compared with the immediate deflection induced by excavation.

Mana and Clough (1981) examined the time effects on lateral wall deflection in several case histories in San Francisco Bay mud. They concluded that higher creep rates are associated with lower factors of safety against basal heave and that the wall deflection rate decreases rapidly with time. In their study, the deflection rates were in the range of 0.3 to 30 mm/d, values much larger than those in this study. The reason for such a difference may be the different stress levels occurring in the soils. Sheet pile was used in Mana and Clough's case histories, where the excavation depth ranged from 9.1 to 13.5 m. The ratios of maximum lateral wall deflection to maximum excavation depth for the case histories observed by Mana and Clough (1981) (0.5% to 3.0%) are generally larger than in the TNEC excavation project (0.5%). The soil near the excavation zone in Mana and Clough's case histories was presumed to be near the failure condition. The stress levels of the soils near the excavation zone in their case histories would be expected to be higher than those in the TNEC case history. A higher stress level of the soils normally produces a higher potential creep behavior. This may account for the larger maximum deflection rates in Mana and Clough's study than in this study and why the deflection rate of the wall in the TNEC excavation project increased with excavation depth.

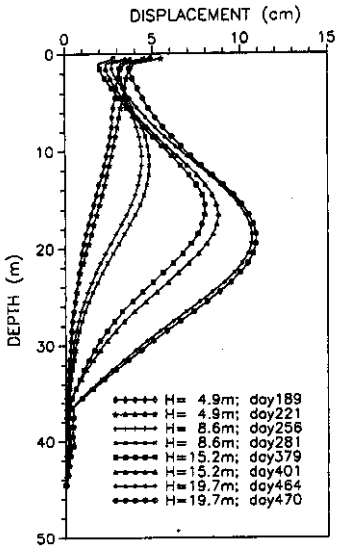

FIG. 8. Variation of Wall Displacement with Time (I-1)

BENDING MOMENT OF DIAPHRAGM WALL

A schematic diagram for computing the bending moment of the diaphragm wall based on measurements from the rebar strainmeters is presented in the insert of Fig. 10. This computation assumes that the variation of stresses over a cross section of the wall is linear. The concrete is assumed to be capable of sustaining a tension force until the tension stress in the concrete exceeds the allowable tension stress. The wall bending moment at various stages can then be obtained on the basis of this computational procedure. Fig. 10 shows the computational results for stages 5, 9, and 13.

The bending moment can also be computed using the equation $M = EI/r$ from the curvature radius of the wall deflection curve, where M is the bending moment of the wall, E is Young's modulus, and I is the moment of inertia. Fig. 10 also shows the wall bending moments at stages 5, 9, and 13 based on wall displacements. This figure shows that the bending moments computed from the rebar strain gauges are generally smaller than those from the wall deflection curve, particularly for the location where the maximum lateral wall deflection occurred and its neighboring location. This is because the bending moment from the wall deflection curve is computed without considering cracking concrete so that the moment of inertia (I) is not reduced. As a matter of fact, some cracks

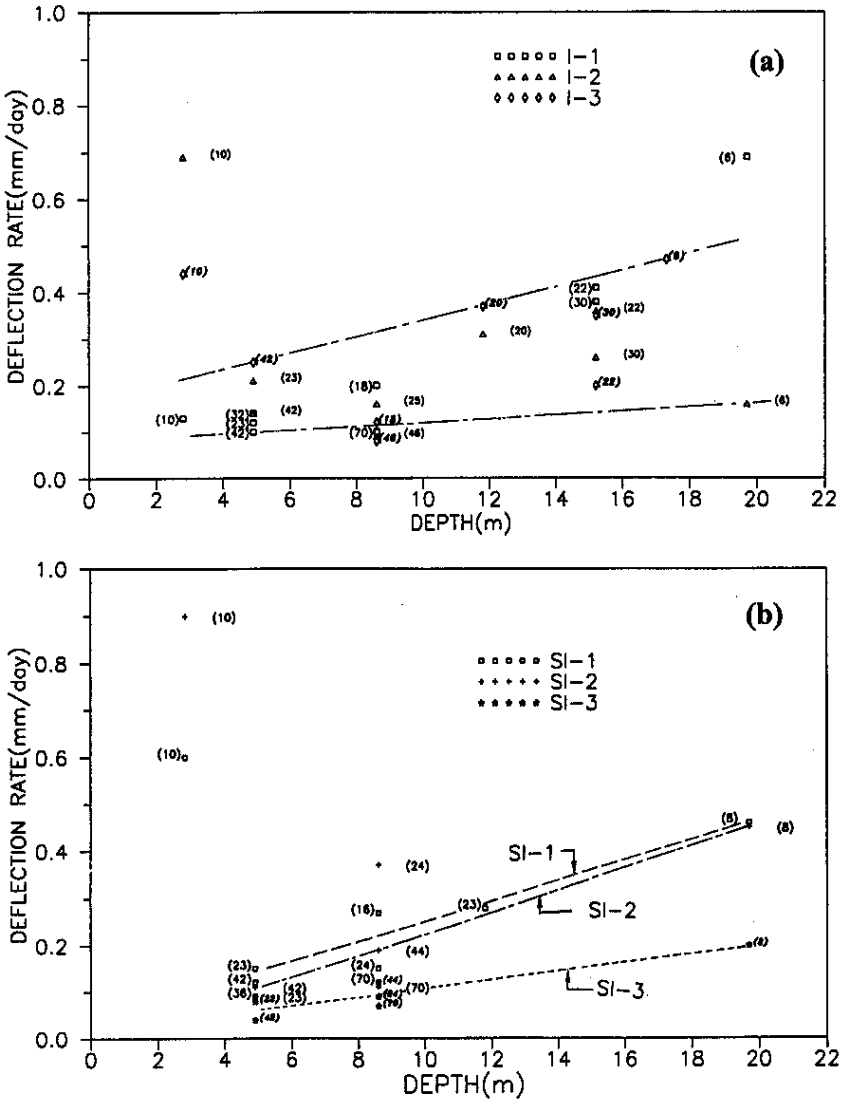

FIG. 9. Variation of Maximum Lateral Deflection Rate of the Wall and Soil with Time, with Numbers in Parentheses Denoting Δt: (a) I-1, I-2, I-3; (b) SI-1, SI-2, SI-3

actually exist in the concrete because of the deformation of the concrete wall, subsequently thereby reducing the moment of inertia. The reduction factor for the moment of inertia (R) is then defined as the ratio of the moment obtained from the rebar strain gauge to the moment obtained from the inclinometer measurement. Fig. 11 presents the variation of the reduction factor with depth for these stages. As shown in this figure, the reduction factor decreases with excavation depth. This information is valuable in the structural design of a diaphragm wall as well as in predicting wall deformations using numerical tools.

LATERAL EARTH PRESSURE ON DIAPHRAGM WALL

The total lateral earth pressures and pore-water pressures acting on the unexcavated side and excavated side of the wall can be obtained by observing the combined earth/water pressure cells. The observation details and complete monitoring results were presented by Ou and Liao (1995). Compared with the theoretical lateral at-rest (K_0) earth pressure prior to excavation, the initial readings were not exactly in the K_0 condition. The theoretical total lateral earth pressure at rest (σ_h) was computed according to the equation $\sigma_h = K_0 \sigma'_v + U$. K_0

TABLE 3. Relationship between Wall Deflections and Time

Depth (m) (1)	Construction day[a] (d) (2)	Δt (d) (3)	Elevation = −10 m: $\Delta\delta/\Delta t$[b] (mm/d) (4)	Elevation = −10 m: $\Delta\delta$ (mm) (5)	Elevation = −20 m: $\Delta\delta/\Delta t$[b] (mm/d) (6)	Elevation = −20 m: $\Delta\delta$ (mm) (7)
4.9	189–233	45	0.09	4.05	0.07	3.15
8.6	256–318	63	0.07	4.41	0.10	6.30
11.8	338–363	26	0.21	5.46	0.31	8.06
15.2	379–409	31	0.16	4.96	0.38	11.78

Note: Accumulated deflection is 18.88 mm at −10 m and 29.29 mm at −20 m.

[a]The range 189–233 denotes construction day 189 to 232, etc.

[b]Values are from Fig. 8.

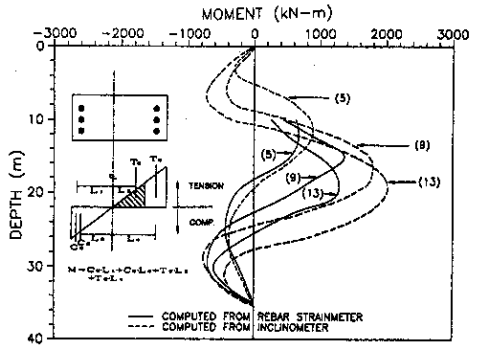

FIG. 10. Comparison of Wall Bending Moments from the Rebar Strain Gauge and the Inclinometer

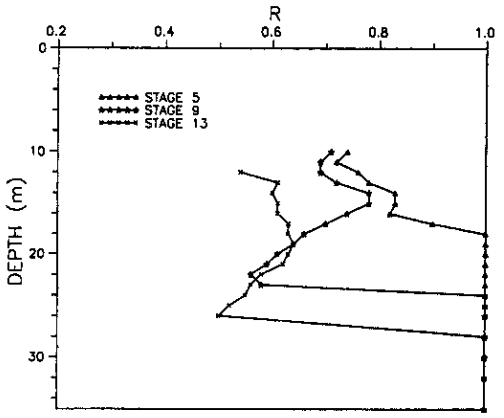

FIG. 11. Variation of Reduction Factor for Wall Bending Moment at Various Stages of Excavation

was computed from Jaky's equation $K_0 = 1 - \sin\phi'$, ϕ' is the drained friction angle; σ'_v is the effective overburden pressure; and U is the pore-water pressure and can be assumed to be the hydrostatic condition.

The difference between theoretical and observed values may occur because the initial readings were affected by the jacking operation while installing the pressure cells to make a good contact with the sidewall of the trench. Strictly speaking, such observed values cannot represent the actual lateral earth pressure at rest (DiBiagio and Roti 1972; Moh and Huang 1993; Karlsrud 1981). If the theoretical K_0 pressure is treated as the actual initial pressure, the observed earth pressure at each stage can thus be adjusted.

Figs. 12(a and b) compare the observed lateral earth pressures (adjusted) and the theoretical Rankine active and passive pressures for stages 3 and 7 and for stages 9 and 13, respectively. As shown in these figures, the lateral earth pressure at the shallow depth (about 12 m) on the unexcavated side increased with excavation depth to the at-rest K_0 condition. This behavior can be accounted for by the fact that the wall had deep inward movement, thereby causing it to rotate at shallow depths and move to the unexcavated side (i.e., push into the soil). For soil at deeper levels, the lateral earth pressure on the unexcavated side decreased with excavation depth to values smaller than theoretical Rankine active earth pressure. As generally known, Rankine's earth pressure would not take into account the friction between the soil and the diaphragm wall. However, trench excavation normally causes a rugged boundary surface between a trench and soil; the diaphragm wall surface would be expected to be rough. Therefore, assuming that no friction exists between the soil and concrete wall will overestimate the lateral earth pressure in the unexcavated side.

As shown in Fig. 12, the observed lateral earth pressure on the excavation side at excavation stage 3 is markedly smaller than the theoretical Rankine passive earth pressure. As described in the preceding section, the maximum wall deflection at this stage, which occurred near the ground surface, was 4.0 cm. This occurrence implies that the magnitude of wall movements does not cause failure of the soil on the excavated side. The amount of difference between the observed and the theoretical value diminished with excavation depth. This difference became small at the final stage (stage 13), except for the

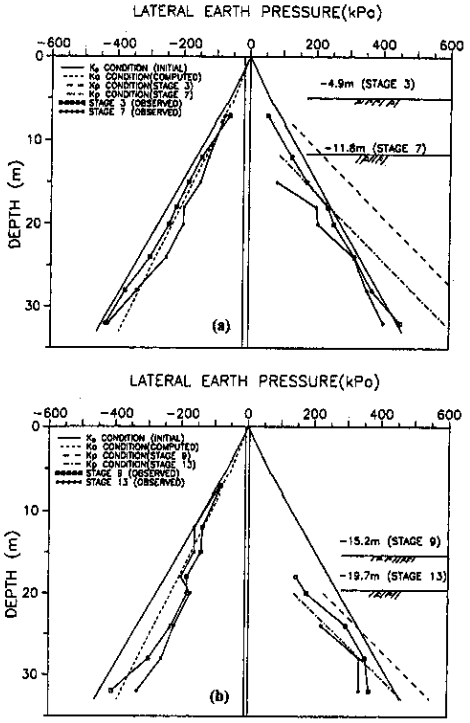

FIG. 12. Observed Lateral Earth Pressure versus Theoretical Rankine Earth Pressure: (a) Stages 3 and 7; (b) Stages 9 and 13

soil at 32.0 m below the ground surface. The soil at this position should be far from the failure condition because the wall deflection at the same level was only 2.8 cm.

PORE-WATER PRESSURE RESPONSE

As shown in Figs. 1 and 2, 35 electronic-type piezometers were installed in the soil on the excavation and the unexcavated sides. Pore-water pressure acting on the wall can be obtained by observing the combined earth/water pressure cells. Some of the measurement results have been presented by Ou and Liao (1995). A more refined discussion is presented herein.

Fig. 13 shows the pore-water pressure contours observed from the piezometers for stages 5 and 13. As shown in this figure, excavation caused the pore-water pressures to decrease with increasing depth and with decreasing distance from the wall. The pore-water pressure in the zone bounded by the horizontal distance greater than 2 m from the wall and by the depth approximately less than the excavation surface (depth = 8.6 m) changed only slightly at stage 5, compared with the preexcavation condition. A similar response was found for stage 13 and the other excavation stages. This can be accounted for the maximum lateral wall deflection occurring near the excavation surface for most of the stages. The soil below the excavation surface, even far from the wall, was subjected to relatively larger shear stresses.

Fig. 13 also reveals that the pore-water pressure contours inside the excavation moved down as excavation proceeded. The decreased pore-water pressure level near the center of the site was larger than that near the wall. The contours at the center part of the excavation zone were nearly horizontal. This is because the decrease of the pore-water pressure was directly affected by releasing the overburden pressure during excavation. The soil near the wall experienced the release of overburden pressure, which caused the pore-water pressure to decrease, as well as lateral compression, which resulted in an increase in pore-water pressure. This occurrence explains why the pore-water pressures near the wall were higher than those at the center part.

Because the excavation was carried out using the top-down construction method, considerable time was required to erect the molds and to pour the concrete floor slab before the next stage of excavation. The pore-water pressure would be expected to change during this period. Fig. 14 shows the variation of pore-water pressure with time. As indicated in this figure, piezometers SP-5 and SP-6 were installed on the wall at a depth of 20 m in the unexcavated and excavated sides, respectively (Fig. 2). Piezometer P1-21 was 21 m below the ground surface and 20.0 m away from the wall inside the excavation. Piezometer P4-20 was 20 m deep and 2.0 m away from the wall outside the excavation. As revealed in this figure, the pore-water pressure dropped significantly during excavation. However, the pore-water pressure gradually increased with time, except for the initial stages. This behavior is attributed to the fact that negative excess pore-water pressures dissipated with time. This observation corresponds to the field observations on wall deflection and settlement, in which the deformation increased with time. Note that there was no dewatering used for this case because the subsurface soil profile within the depth of excavation was composed mainly of cohesive soil.

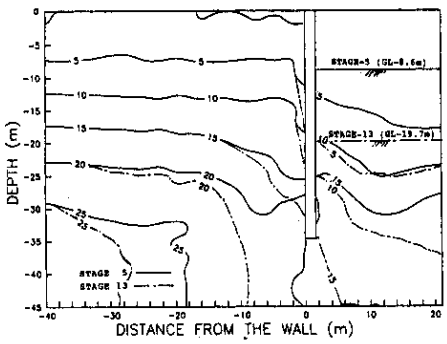

FIG. 13. Variation of Pore-Water Pressure (Expressed in kPa) Inside and Outside the Excavation

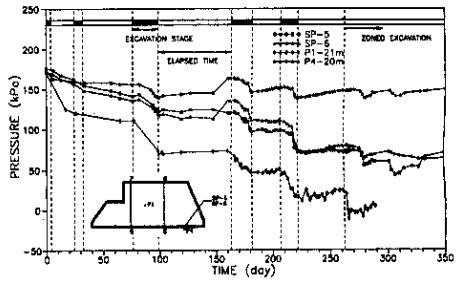

FIG. 14. Variation of Pore-Water Pressure with Time

GROUND SURFACE SETTLEMENT

Fig. 15 shows the ground surface settlement profile at the main observation section at key excavation stages. As revealed in this figure, the settlement increased with excavation depth. The maximum ground surface settlement after the completion of the final excavation stage (stage 13, excavation depth = 19.7 m) was 7.8 cm. The ratios of maximum ground surface settlement to maximum horizontal wall deflection at all excavation stages ranged from 0.56 to 0.78, which are generally within the range of the findings by Clough and O'Rourke (1990).

The maximum ground surface settlement occurred near the diaphragm wall at the first stage. This occurrence is perhaps attributed to the fact that the wall behaved like a cantilever at this stage. As the excavation proceeded, the maximum ground surface settlement occurred at some distance behind the wall. The ratios of the location of the maximum surface settlement behind the wall to the depth where the maximum lateral wall deflection occurred are in the range of 0.63 and 0.78. This value is larger than observations by Nicholson (1987). Note from Fig. 7(a) that deep inward movement began to develop on the wall after stage 3, which may account for the maximum surface settlement occurring at some distance from the wall at these stages.

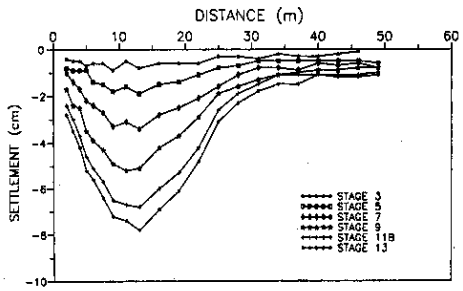

FIG. 15. Settlement Profiles Induced by Excavation

As shown in Fig. 15, the soil movement extended to a considerable distance behind the wall. The soil settled 1.2 cm even at a distance of 49 m from the wall. In other words, the influence zone caused by excavation may be more than 49 m. Buildings or facilities within the influence zone could be damaged, depending on the degree of distortion and the condition of the structures. The apparent influence range (AIR) was then defined as the horizontal distance behind the wall to the location where the settlement becomes uniform (Ou et al. 1993). As shown in this figure, the AIR does not vary with excavation depth. The magnitude of the AIR for each stage was roughly 30 m. This value is slightly larger than that calculated from the equation AIR = L tan (45° − ϕ/2) (Ou et al. 1993), where L is the depth of diaphragm wall and ϕ is the friction angle of the soil.

Fig. 16(a) presents the relationship between normalized settlement and distance from the wall for the final excavation stage. This figure also contains the three categories of typical excavation performance defined by Peck (1969). Field observation results indicate that the relationship for the final stage falls into category I, although Peck's categories were established for excavations with braced sheet-pile walls or soldier piles with laggings, which differ markedly from the case history presented herein. Fig. 16(b) shows the relationship between normalized settlement (δ_v/δ_{vm}) at various distances and normalized distance from the wall (d/H) for the key stages. As indicated in this figure, the normalized settlement also falls inside the envelope identified by Clough and O'Rourke (1990).

Fig. 17 shows the ground surface settlement profile as a function of time for some stages. As shown in this figure, the ground surface settlement also increased with time while the excavation depth remained unchanged. As stated in the preceding section, both effects of soil creep and excess pore-water pressure dissipation may partially contribute to some extent because considerable time is normally required for the top-down construction method. Fig. 18 shows the relationship between settlement rates ($\Delta S/\Delta t$) at a distance of 13 m from the wall and excavation depth. As shown in this figure, the settlement rate increased with excavation depth. The settlement rates were in the range of 0.1 mm/d to 0.4 mm/d.

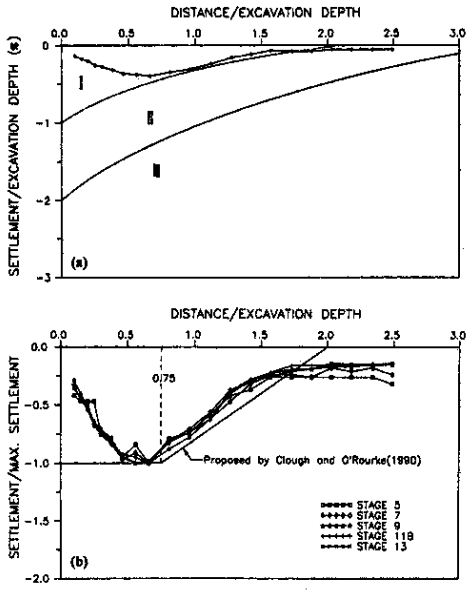

FIG. 16. Observed Settlement Profile versus Computed Settlement Profile Using Empirical Methods: (a) Final Excavation Stage; (b) Key Stages

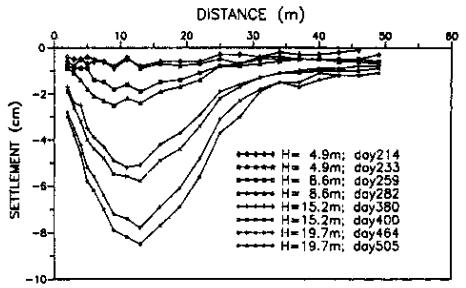

FIG. 17. Variation of Ground Surface Settlement with Time

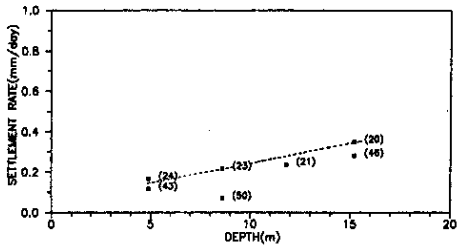

FIG. 18. Variation of Settlement Rate for Soil 13 m from Wall with Time, with Numbers in Parentheses Denoting Δt

TABLE 4. Relationship between Ground Surface Settlement and Time

Depth (m) (1)	Construction day[a] (d) (2)	Δt (d) (3)	$\Delta S/\Delta t$[b] (mm/d) (4)	ΔS (mm) (5)
4.9	189–233	45	0.116	5.22
8.6	256–318	63	0.10	6.30
11.8	338–363	26	0.238	6.19
15.2	379–419	22	0.350	7.70

Note: Accumulated settlement is 25.41 mm.
[a]The range 189–233 denotes construction day 188 to 232, etc.
[b]Values are from Fig. 17.

Table 4 shows the settlement at a distance of 13 m from the wall during the periods when the excavation depths remained unchanged from the beginning of excavation to the end of stage 10. As shown in this table, the accumulated settlement (S_1) during the periods when the excavation depths remained unchanged was 25.41 mm; the corresponding total settlement (S_2) was 58 mm (Fig. 15). The ratio of S_1 to S_2 is 44%. This ratio was fairly large compared with the immediate settlement induced by excavation.

EXCAVATION BOTTOM HEAVE

Very limited field observations regarding heave at the excavation surface have been reported in the literature. As indicated in Fig. 2, a heave gauge was installed at 20 m from the southern wall at a depth of 21.5 m below the ground surface (maximum excavation depth = 19.7 m). Fig. 19 shows the variation of bottom heave with excavation depth. The arabic number in parentheses in the figure denotes the period of

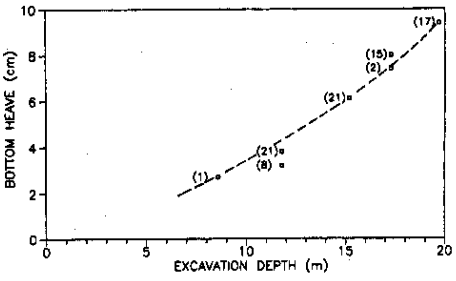

FIG. 19. Variation of Excavation Bottom Heave with Depth, with Numbers in Parentheses Denoting Δt

the excavation depth remaining unchanged. As excavation proceeded to the final stage, the magnitude of the heave at excavation bottom was equal to 9.7 cm. The ratio of bottom heave to maximum ground surface settlement for each stage is in the range of 0.94 to 1.42. The implications of the bottom heave with respect to the conditions of an excavation require further study.

CONCLUSIONS

This paper presents the characteristics of movements of the diaphragm wall and soil caused by the TNEC excavation project using the top-down construction method. The behavior of the diaphragm wall and soil with time was also studied. Records of construction activities as well as observations of excavation performance were fairly complete. Therefore, these observations may not only facilitate a more thorough understanding of the general excavation behavior, but also provide a good case history to calibrate and verify numerical tools. In addition, the following observations and conclusions can be made on the basis of the work presented herein:

1. According to the field observations, the observed strut loads were close to the values computed using Peck's apparent earth pressure diagram for the average undrained shear strength used. For the struts close to the excavation corners, the load in the strut was relatively small. The corner effects apparently had a significant effect on the strut loads.
2. The maximum horizontal displacement of an inclinometer casing 2 m away from the wall was close to that of the wall. Deep inward movements developed for the wall as well as the soil near the wall. This behavior became less pronounced with increasing horizontal distance from the wall. The maximum lateral wall displacement occurred near the excavation surface. The ratio of maximum lateral wall displacement to excavation depth ranged from 0.51% to 0.57%, except for the initial excavation stages.
3. The ratio of the wall bending moment obtained from the rebar strain gauges to the moment obtained from the inclinometer measurements decreased with increasing excavation depth. This response may be because some cracks exist in the concrete wall as a consequence of the deformation of the concrete wall. Therefore, the structural design of the diaphragm wall as well as the prediction of the wall deformation should consider this factor.
4. Field observations indicated that the lateral earth pressure at shallow depths (i.e., less than about 12.0 m) on the unexcavated side increased with excavation depth to the at-rest K_0 condition because the wall had deep inward movement, which caused it to push toward the soil at shallow depth. For the soil at deeper levels, the lateral earth pressure on the unexcavated side decreased with excavation depth to values smaller than the theoretical Rankine active earth pressure. This behavior can perhaps be attributed to the fact that, for Rankine's earth pressure theory, no friction between the wall and soil is considered.
5. The influence range caused by excavation extended to a considerable distance from the wall. However, the apparent influence range, where the building may be affected by the excavation, was equal to about 30.0 m. This value did not vary with excavation stage. The maximum ground surface settlement occurred at a distance 0.63 to 0.78 times the depth where maximum lateral wall deflection occurred. This value also did not vary with excavation depth. The normalized settlement profile with respect to the maximum value was in good agreement with Clough and O'Rourke's studies. The normalized settlement profile with respect to the final excavation depth was near the boundary of zones I in Peck's diagram. The magnitude of the bottom heave was equal to 9.7 cm at the final excavation depth. The ratio of bottom heave to maximum ground surface settlement was in the range of 0.94 to 1.42
6. Wall deflection and settlement generally increased with time while the excavation depth remained unchanged. The magnitudes of the deflection and settlement rates increased with an increasing excavation depth. In this project, the maximum deflection rate was in the range of 0.1 to 0.6 mm/d. The effects of both soil creep and excess pore-water pressure dissipation may partially contribute to this behavior. As excavation proceeded to a depth of 15.2 m, the percentage of accumulated wall deflection at depths of 10 and 20 m during the periods when the excavation depths remained unchanged were 30% and 36%, respectively. The percentage of settlement for the soil at a distance of 13 m from the wall was 44%. These percentages were fairly large compared with the immediate deformation induced by excavation. Therefore, analysis of excavation in soft clay should consider the creep factors and/or pore-water pressure dissipation.
7. The pore-water pressure in the soil outside the excavation decreased significantly, except for the soil near the wall and above the excavation surface. The magnitude of the pore-water pressure decrease near the center of the site was less than that near the wall. This response is due to the soil near the wall experiencing the release of overburden pressure as well as the lateral compression of the wall. The pore-water pressure dropped significantly during the period of excavation. However, pore-water pressures gradually increased with time, except for the initial stages. This phenomenon was consistent with the field observations on wall deflection and settlement, in which the movements increased with time.

ACKNOWLEDGMENTS

The writers would like to thank the National Science Council at Taiwan for financial support of this research work under Contract No. NSC82-0410-E011-23.

APPENDIX I. REFERENCES

Clough, G. W., and O'Rourke, T. D. (1990). "Construction-induced movements of insitu walls." *Proc., Design and Performance of Earth Retaining Structure*, ASCE, Reston, Va., 439–470.

DiBiagio, E., and Roti, J. A. (1972). "Earth pressure measurements on a braced slurry-trench wall in soft clay." *Proc., European Conf. on Soil Mech. and Found. Engrg.*, 473–483.

Finno, R. J., Atmatzidis, D. K., and Perkins, S. B. (1989). "Observed

performance of a deep excavation in clay." *J. Geotech. Engrg.*, ASCE, 115(8), 1045–1064.
Finno, R. J., and Nerby, S. M. (1989). "Saturated clay response during braced cut construction." *J. Geotech. Engrg.*, ASCE, 115(8), 1065–1084.
Karlsrud, K. (1981). "Performance and design of slurry walls in soft clay." *Proc., ASCE Spring Convention*, ASCE, Reston, Va.
Mana, A. I., and Clough, G. W. (1981). "Prediction of movements for braced cut in clay." *J. Geotech. Engrg. Div.* ASCE, 107(8), 759–777.
Mesri, G. (1973). "Coefficient of secondary compression." *J. Soil Mech. and Found. Div.*, ASCE, 121–137.
Moh, Z. C., and Hawang, R. N. (1993). "Earth pressures on walls of a deep excavation." *Proc., 3rd Int. Conf. on Case Histories in Geotech. Engrg.*, 1–5.
Nicholson, D. P. (1987). "The design and performance of the retaining wall at Newton Station." *Proc., Singapore Mass Rapid Transit Conf.*, 147–154.
Ou, C. Y., Hisieh, P. G., and Chiou, D. C. (1993). "Characteristics of ground surface settlement during excavation." *Can. Geotech. J.*, Ottawa, Canada, 30(5), 758–767.
Ou, C. Y., and Liao, J. T. (1995). "Variations of earth and porewater pressures during deep excavation." *J. Chinese Inst. of Civ. and Hydr. Engrg.*, 7(3), 253–262.
Peck, R. B. (1969). "Deep excavation and tunneling in soft ground." *Proc., 7th Int. Conf. on Soil Mech. and Found. Engrg.*, 225–290.
Robertson, P. K., and Campanella, R. G. (1989). "Guidelines for geotechnical design using the cone penetrometer test and CPT with pore pressure measurement." Hogentogler Co., Inc.
Singh, A., and Mitchell, J. K. (1968). "General stress-strain-time function for soils." *J. Soil Mech. and Found. Div.*, ASCE, 94(1), 21–46.

APPENDIX II. NOTATION

The following symbols are used in this paper:

A_1, m, α = Singh and Mitchell's creep parameters;
c = cohesion intercept;
C_c = compressive force in concrete;
C_s = compressive force in steel;
T_c = tension force in concrete;
T_s = tension force in steel;
c_v = coefficient of consolidation;
E = Young's modulus;
H = depth of excavation;
I = moment of inertia;
k = coefficient of permeability;
K_0 = coefficient of lateral earth pressure at rest;
L = depth of diaphragm wall;
M = bending moment of wall;
N_k = empirical cone factor;
R = reduction factor for moment of inertia;
U = pore-water pressure;
Δt = period during which excavation depth remained unchanged;
δ_1 = accumulated deflection during periods when excavation depths remained unchanged;
δ_2 = total deflection;
$\Delta\delta/\Delta t$ = deflection rate;
S_1 = accumulated settlement during periods when excavation depths remained unchanged;
S_2 = total settlement;
$\Delta S/\Delta t$ = settlement rate;
ϕ' = drained friction angle;
ε_s = coefficient of secondary consolidation;
σ'_v = effective overburden pressure;
σ_h = total lateral earth pressure;
δ_v = ground surface settlement behind wall; and
δ_{vm} = maximum ground surface settlement.